Supporting Information: Force-dependent unbinding rate of molecular motors from stationary optical trap data

Florian Berger,[*,†] Stefan Klumpp,[‡] and Reinhard Lipowsky[¶]

Laboratory of Sensory Neuroscience, The Rockefeller University, New York, 10065 NY, USA, Institute for the Dynamics of Complex Systems, Georg-August University Göttingen, 37077 Göttingen, Germany, and Theory & Bio-Systems, Max Planck Institute of Colloids and Interfaces, 14424 Potsdam, Germany

E-mail: fberger@rockefeller.edu

The probability density function of unbinding forces

For our distribution-based analysis we derive analytical expressions for the probability density function of unbinding forces for three different force-dependent bond behaviors.

[*]To whom correspondence should be addressed

[†]Laboratory of Sensory Neuroscience, The Rockefeller University, New York, 10065 NY, USA

[‡]Institute for the Dynamics of Complex Systems, Georg-August University Göttingen, 37077 Göttingen, Germany

[¶]Theory & Bio-Systems, Max Planck Institute of Colloids and Interfaces, 14424 Potsdam, Germany

The slip bond

We describe a slip bond with an unbinding rate that increases with the trapping force as

$$\epsilon(F_\mathrm{t}) \equiv \epsilon_0 \exp(F_\mathrm{t}/F_\mathrm{d}). \tag{S 1}$$

Here, we introduce the force-free unbinding rate ϵ_0 and the characteristic detachment force F_d. To calculate the corresponding distribution of unbinding forces, we proceed as explained in the main text and find

$$p(F) = \frac{F_\mathrm{s}\epsilon_0 \exp[F/F_\mathrm{d}]}{\kappa_\mathrm{eff} v_0 (F_\mathrm{s} - F)} \exp\left[-\frac{\epsilon_0 \exp[F_\mathrm{s}/F_\mathrm{d}] F_\mathrm{s}}{\kappa_\mathrm{eff} v_0} \left(I\left(\frac{F_\mathrm{s} - F}{F_\mathrm{d}}\right) - I\left(\frac{F_\mathrm{s}}{F_\mathrm{d}}\right)\right)\right], \tag{S 2}$$

with the exponential integral function

$$I(x) \equiv \int_x^\infty t^{-1} \exp[-t] dt. \tag{S 3}$$

This equation implies that we cannot obtain v_0, κ_eff and ϵ_0 independently from a fit, only the combination

$$F_\mathrm{c} \equiv \frac{v_0 \kappa_\mathrm{eff}}{\epsilon_0} \tag{S 4}$$

that defines the characteristic force F_c. We simplify the distribution to

$$p(F|F_\mathrm{c}, F_\mathrm{d}, F_\mathrm{s}) = \frac{F_\mathrm{s} \exp[F/F_\mathrm{d}]}{F_\mathrm{c}(F_\mathrm{s} - F)} \exp\left[-(F_\mathrm{s}/F_\mathrm{c}) \exp[F_\mathrm{s}/F_\mathrm{d}] \left(I\left(\frac{F_\mathrm{s} - F}{F_\mathrm{d}}\right) - I\left(\frac{F_\mathrm{s}}{F_\mathrm{d}}\right)\right)\right], \tag{S 5}$$

which depends now on the three parameters, F_c, F_d, and F_s.

The slip-ideal bond

An ideal bond is characterized by a constant unbinding rate that is independent of the force.[1,2] As a phenomenological description for a slip-ideal bond with an unbinding rate that first increases with force and then becomes constant, we use the rational function

$$\epsilon(F_\mathrm{t}) \equiv \frac{\epsilon_0 F_\mathrm{t}}{F_\mathrm{a} + F_\mathrm{t}}. \tag{S 6}$$

The corresponding distribution for the unbinding forces follows as

$$p(F|F_\mathrm{a}, F_\mathrm{c}, F_\mathrm{s}) = \frac{F F_\mathrm{s}}{F_\mathrm{c}(F_\mathrm{a}+F)(F_\mathrm{s}-F)} \exp\left(\frac{F_\mathrm{s}}{F_\mathrm{c}(F_\mathrm{a}+F_\mathrm{s})}\left(F_\mathrm{a}\ln\left(1+\frac{F}{F_\mathrm{a}}\right) + F_\mathrm{s}\ln\left(1-\frac{F}{F_\mathrm{s}}\right)\right)\right), \tag{S 7}$$

in which F_c is the characteristic force given in Eq. S 4.

The catch bond

A catch bond is characterized by an unbinding rate that decreases with increasing force.[1] We describe such a bond with the force-dependent unbinding rate

$$\epsilon(F_\mathrm{t}) = \epsilon_0 \exp(-F_\mathrm{t}/F_\mathrm{d}) + a. \tag{S 8}$$

The corresponding distribution of unbinding forces reads

$$\begin{aligned} p(F|F_\mathrm{a}, F_\mathrm{c}, F_\mathrm{d}, F_\mathrm{s}) = \\ &\frac{F_\mathrm{s}(F_\mathrm{c}/F_\mathrm{a} + \exp[-F/F_\mathrm{d}])}{F_\mathrm{c}(F_\mathrm{s}-F)} \exp\Bigg[(F_\mathrm{s}/F_\mathrm{c})\exp[-F_\mathrm{s}/F_\mathrm{d}]\left(I\left(-\frac{F_\mathrm{s}}{F_\mathrm{d}}\right) - I\left(\frac{F-F_\mathrm{s}}{F_\mathrm{d}}\right)\right) + \\ &(F_\mathrm{s}/F_\mathrm{a})(\ln(1-F/F_\mathrm{s})\Bigg)\Bigg], \end{aligned} \tag{S 9}$$

in which F_c is defined in Eq. S 4 and $F_\mathrm{a} \equiv v_0\kappa_\mathrm{eff}/a$.

Simulations

To generate data for the validation of our methods, we assume that the motor steps forward with $\ell = 8\,\mathrm{nm}$ steps with a force-dependent stepping rate $\alpha(F_\mathrm{t})$. We relate the stepping rate

$$\alpha(F_\mathrm{t}) = v(F_\mathrm{t})/\ell = v_0(1 - F_\mathrm{t}/F_\mathrm{s})/\ell \tag{S 10}$$

to a linear force velocity $v(F_\mathrm{t})$ described by the stall force $F_\mathrm{s} \simeq 6\,\mathrm{pN}$ and a typical force-free velocity $v_0 \simeq 1\,\mu\mathrm{m/s}$. For studying the different unbinding behaviors we use the corresponding unbinding rates $\epsilon(F_\mathrm{t})$, introduced above and listed in Table S1. The stepping and unbinding of the motor are force-dependent and the force on the motor changes as it pulls the bead out of the center of the optical trap. To determine the force exerted on the motor, we assume a linear restoring force of the optical trap, characterized by a typical trap stiffness of $\kappa_\mathrm{t} \simeq 0.01\,\mathrm{pN/nm}$ and a linear force-extension relation for the motor molecule with spring constant $\kappa_\mathrm{m} \simeq 0.3\,\mathrm{pN/nm}$.[3] The trapping force

$$F_\mathrm{t} = \kappa_\mathrm{t} x_\mathrm{b} \tag{S 11}$$

on the bead is determined from the distance x_b of the bead to the center of the trap. This distance changes with the position x_m of the motor, while it is moving out of the center of the trap, as

$$x_\mathrm{b} = \frac{\kappa_\mathrm{m}}{\kappa_\mathrm{m} + \kappa_\mathrm{t}} x_\mathrm{m}. \tag{S 12}$$

Under the assumption that after each step the system reaches mechanical equilibrium instantaneously, the force on the bead equals the force on the bond of the motor and the filament with the corresponding loading rate

$$\dot{F}_\mathrm{t} = \kappa_\mathrm{t} \frac{\kappa_\mathrm{m}}{\kappa_\mathrm{m} + \kappa_\mathrm{t}} \dot{x}_\mathrm{m}. \tag{S 13}$$

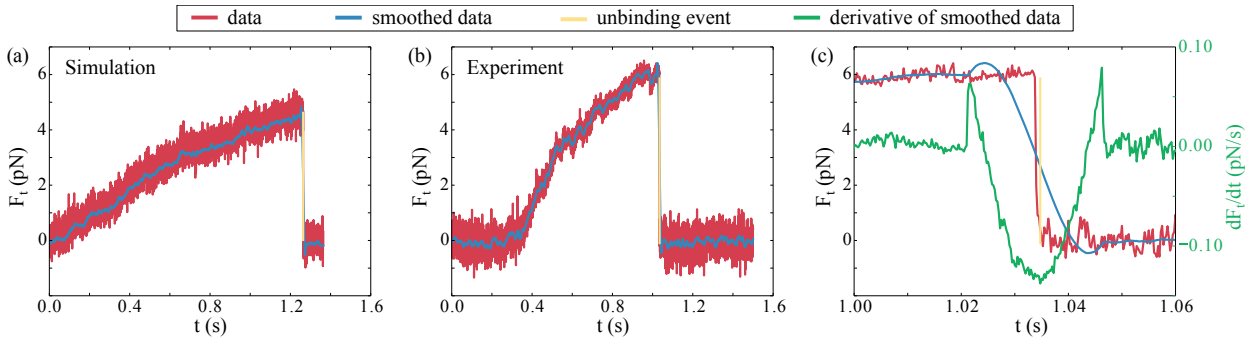

Figure S1: **Analysis of force traces** The original trapping-force traces F_t as a function of time t (red) from the simulations and experiments are smoothed with a Savitzky-Golay filter (blue) and one example for each are shown in (a) and (b) respectively. Our unbinding detection algorithm determines the magnitude of the unbinding force (yellow) and displays it close to the unbinding event to allow for visual inspection. To explain the basic idea of the algorithm, we magnified the unbinding event of (b) in (c) and show the derivative as the discrete difference (green) between points of the smoothed force trace. The location of the two maxima of the derivative are reliable estimates of time points before and after the unbinding event. Taking the difference of the averages of the traces before and after the unbinding event provides the numerical value for the unbinding force.

We base our stochastic simulation on a Gillespie algorithm: at each step we calculate the force acting on the motor, adjust the stepping and unbinding rates accordingly and choose the next event with the corresponding probability.[4] If the motor steps forward, we increase the position x_m by the step size ℓ. If the motor unbinds from the filament, we set the position to $x_\mathrm{m} = 0$. In this way, we obtain trajectories of a single molecular motor as it pulls the bead out of a stationary trap. We convert the spatial trajectories corresponding to the bead position as a function of time into force traces by multiplying the bead position with the stiffness of the trap. To mimic the experimental force traces as closely as possible, we add Gaussian white noise with a standard deviation of $\sigma = 0.3\,\mathrm{pN}$, as estimated from the experimental data. An example of such a force trace is shown in Fig. S1(a).

Detection of unbinding forces from the force traces

The experiments and the simulations provide long force traces with hundreds of binding and unbinding events. From these traces we separate each force-generation event with its associated unbinding event into a separate file, see Fig. S1. We smooth the traces with a Savitzky-Golay filter and take the average of the first 200 points to determine the baseline that we then subtract from the trace. The base line subtraction is not necessary for the simulated traces. From the smoothed trace the position of the unbinding event is automatically detected in the following way; First, we estimate the derivative of the trace as the finite difference between adjacent points, see Fig. S1(c). Then, the jump of the trace after the unbinding event is identified at the time with the smallest derivative. We estimate the numerical value for the unbinding force as the difference of the trace before and after the jump. To obtain an exact value, we need to estimate the time when the unbinding event occurs and when the bead is equilibrated in the center of the trap. Therefore, we start at the time at which the derivative is negative and determine the two nearest time points when the derivative is positive. One point corresponds to a time before the unbinding event and the other point indicates that the bead is equilibrated at the center of the trap. We average 20 data points before the first time point and 20 data points after the equilibration. The difference of these averages provides the numerical value of the unbinding force. We visually inspect each trace and monitor the results of the detection algorithm. In this way we obtain the set of all unbinding forces.

Fitting of the distributions

To determine the numerical values of the free parameters for a specific unbinding behavior, we fit the expressions of the distributions of unbinding forces to either experimental or simulated data. Because fitting the probability densities directly to a histogram constructed

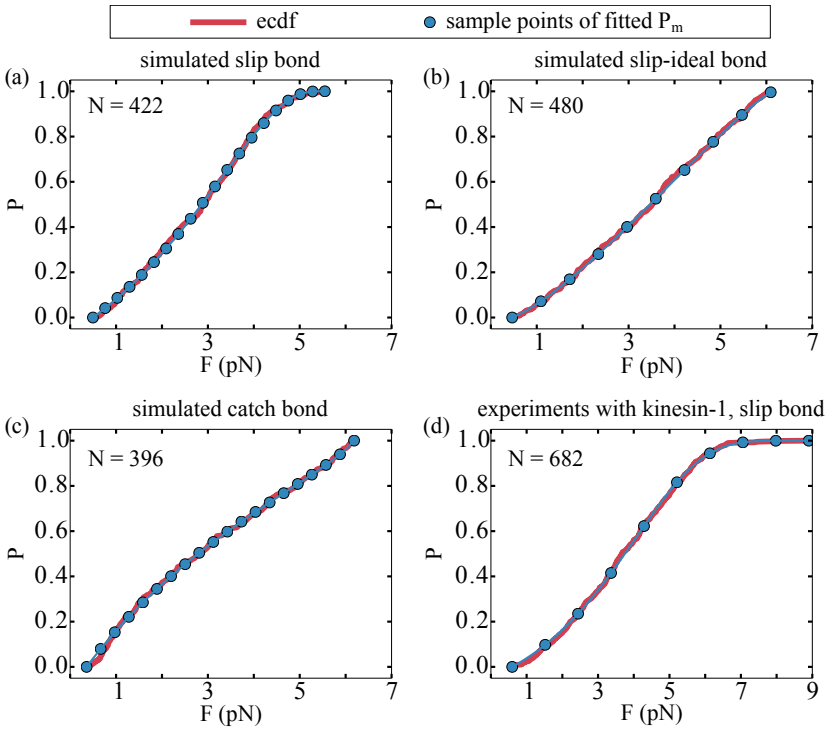

Figure S2: **Fitted probabilities P** The red lines represent the empirical cumulative distribution functions (ecdf) constructed from simulation data of (a) slip bonds, (b) slip-ideal bonds, (c) catch bonds, and (d) from experimental data for kinesin-1. As explained in the text, we fit each ecdf by the cumulative distribution function P_{m} of Eq. S 15 for the respective bond behavior. To enhance the minimization algorithm, we evaluate the integrals of the cdf at a finite number of sample points shown as the blue dots.

from the data depends on the arbitrary choice of the number of bins, we instead fit the cumulative distribution functions (cdf) to empirical cumulative distribution functions (ecdf) constructed from the data. For a data set of N data points, the ecdf is a step function that increases by $1/N$ at each of the N data points. The cumulative distribution function is defined as

$$P(F) \equiv \int_0^F p(F')\, dF'. \tag{S 14}$$

$P(F)$ is a probability and attains values between 0 and 1. To account for the limited resolution of detecting unbinding events in the experiments, we shift and renormalize the

cdfs with respect to the smallest detected unbinding force F_{min} of each data set to

$$P_{\mathrm{m}}(F) \equiv \frac{P(F) - P(F_{\mathrm{min}})}{1 - P(F_{\mathrm{min}})}. \tag{S 15}$$

For our fitting procedure, we evaluate the integrals in the cdfs only for a finite number of sample points $\{F_i\}$. In the case of the slip-bond data with $N = 422$ detected unbinding events, we find the optimal numerical values of the parameters from the minimization

$$\min_{F_{\mathrm{c}},F_{\mathrm{d}},F_{\mathrm{s}}} \sum_i \left(\mathrm{ecdf}(F_i) - P_{\mathrm{m}}(F_i|F_{\mathrm{c}}, F_{\mathrm{d}}, F_{\mathrm{s}})\right)^2, \tag{S 16}$$

in which $P_{\mathrm{m}}(F|F_{\mathrm{c}}, F_{\mathrm{d}}, F_{\mathrm{s}})$ is given from combining Eq. S 5, Eq. S 14, and Eq. S 15. To enhance the performance of the minimization routine in Mathematica, we restrict the intervals for the parameters to $F_{\mathrm{c}} \in (0, +\infty)\,\mathrm{pN}$, $F_{\mathrm{d}} \in (0, 10)\,\mathrm{pN}$, and $F_{\mathrm{s}} \in (0, 10)\,\mathrm{pN}$. We evaluate the integrals at 20 equidistant sample points $\{F_i\}$, see blue dots in Fig. S2. From this fitting procedure, we obtain $F_{\mathrm{c}} \simeq 8.32\,\mathrm{pN}$, $F_{\mathrm{d}} \simeq 3.85\,\mathrm{pN}$, and $F_{\mathrm{s}} \simeq 5.41\,\mathrm{pN}$. With $v_0 \simeq 1000\,\mathrm{nm/s}$, $\kappa_{\mathrm{m}} \simeq 0.3\,\mathrm{pN/nm}$ and $\kappa_{\mathrm{t}} \simeq 0.01\,\mathrm{pN/nm}$, we determine the force-free unbinding rate

$$\epsilon_0 = \frac{v_0 \kappa_{\mathrm{m}} \kappa_{\mathrm{t}}}{F_{\mathrm{c}}(\kappa_{\mathrm{m}} + \kappa_{\mathrm{t}})} \simeq 1.16\,\mathrm{s}^{-1}. \tag{S 17}$$

We obtain 95% confidence intervals with a significance of 0.05 from a bootstrapping procedure. We resample 200 data sets of the original size $N = 422$. For each set we determine the optimal fit parameters and calculate the lower and upper confidence interval as the 2.5 percentile and the 97.5 percentile of the distribution of each fit parameter, respectively. All parameter values are listed in Table S1.

We proceed in the same way for the slip-ideal bond for which we identify $N = 489$ unbinding events in the simulated data. During the minimization, we restrict the parameters to $F_{\mathrm{a}} \in (0.5, 10)\,\mathrm{pN}$, $F_{\mathrm{c}} \in (1, 5)\,\mathrm{pN}$, and $F_{\mathrm{s}} \in (1, 10)\,\mathrm{pN}$. We evaluate the integrals at 10

equidistant sample points $\{F_i\}$, see blue dots in Fig. S2. The numerical values for the optimal parameters are listed in Table S1 with confidence intervals calculated in the same way as for the slip bond.

In the case of the catch bond, we determine the fit parameters as explained for the slip bond above. Our simulated data set contains $N = 396$ unbinding events. To enhance the minimization, we restrict the parameter to: $F_\mathrm{a} \in (0, 20)\,\mathrm{pN}$, $F_\mathrm{c} \in (0, 20)\,\mathrm{pN}$, $F_\mathrm{d} \in (0, 20)\,\mathrm{pN}$, and $F_\mathrm{s} \in (0, 20)\,\mathrm{pN}$. We evaluate the integrals at 20 equidistant sample points $\{F_i\}$, see blue dots in Fig. S2. The optimal numerical values for the free parameters are listed in Table S1 with the 95% confidence intervals determined as for the two other cases.

Table S1: **Validation of distribution-based method:** Each bond behavior is described by the unbinding rate $\epsilon(F_\mathrm{t})$ as given in the first column, depending on three or four parameters as listed in the second column. We choose numerical values for these parameters to generate data from our stochastic simulation. By fitting the expressions for the unbinding-force distributions to the generated data, we estimate the numerical values. The 95% confidence intervals are obtained from bootstrapping.

bond behavior	parameter	value for the simulation	value from fit	CI
slip bond	$\epsilon_0\,(\mathrm{s}^{-1})$	1	1.16	[0.91; 1.62]
$\epsilon(F_\mathrm{t}) = \epsilon_0 \exp(F_\mathrm{t}/F_\mathrm{d})$	$F_\mathrm{d}\,(\mathrm{pN})$	6	3.85	[2.51; 10.00]
	$F_\mathrm{s}\,(\mathrm{pN})$	6	5.41	[4.76;6.45]
slip-ideal bond	$\epsilon_0\,(\mathrm{s}^{-1})$	2	2.11	[1.94; 3.06]
$\epsilon(F_\mathrm{t}) = \epsilon_0 F_\mathrm{t}/(F_\mathrm{a} + F_\mathrm{t})$	$F_\mathrm{a}\,(\mathrm{pN})$	1	0.84	[0.5; 5.78]
	$F_\mathrm{s}\,(\mathrm{pN})$	6	6.13	[3; 6.28]
catch bond	$\epsilon_0\,(\mathrm{s}^{-1})$	3	1.86	[0.86; 3.17]
$\epsilon(F_\mathrm{t}) = \epsilon_0 \exp(-F_\mathrm{t}/F_\mathrm{d}) + a$	$a\,(\mathrm{s}^{-1})$	0.5	0.75	[0.48; 1.51]
	$F_\mathrm{d}\,(\mathrm{pN})$	3	4.18	[0.63; 10.34]
	$F_\mathrm{s}\,(\mathrm{pN})$	6	6.19	[2.28; 6.26]

Trace-based method

We estimate the force-dependent unbinding rate from the traces binned into N force bins with bin width ΔF. We label the bins with k, count the number C_k^un of unbinding events

and the number C_k^{to} of points of all traces in bin k. Intuitively, C_k^{to} is the total number of possible unbinding events and C_k^{un} is the number of actual unbinding events. Thus, the ratio

$$\frac{C_k^{\mathrm{un}}}{C_k^{\mathrm{to}}} \tag{S 18}$$

gives the probability of unbinding in the kth bin at each sampling point in time. We divide this expression by the time step δt between the samples to obtain the unbinding rate

$$\epsilon((k-0.5)\Delta F) = \frac{C_k^{\mathrm{un}}}{\delta t C_k^{\mathrm{to}}}. \tag{S 19}$$

Note, the denominator $\delta t C_k^{\mathrm{to}}$ is equal to the total time of all traces spent in the kth bin. This expression has been used previously to estimate the unbinding rate of molecular motors.[3,5] In the following, we rewrite this estimator for the unbinding rate to obtain the estimator introduced by Dudko et al.[6] The number of unbinding events per bin is related to the density histogram h_k as

$$C_k^{\mathrm{un}} = N^{\mathrm{un}} \Delta F h_k, \tag{S 20}$$

in which N^{un} is the total number of all unbinding events. To approximate the total time that the traces spent in the kth bin, we first look at all traces that pass through the bin without unbinding. The number of these traces is given by all traces that unbind after bin k, i.e.,

$$\sum_{i=k+1}^{N} C_i^{\mathrm{un}}. \tag{S 21}$$

Multiplying this number by the mean time spent in the bin provides the total time of all traces passing through that bin as

$$\delta t \left\langle N_k^{\mathrm{to}} \right\rangle \sum_{i=k+1}^{N} C_i^{\mathrm{un}}, \tag{S 22}$$

in which $\langle N_k^{\mathrm{to}} \rangle$ is the mean number of data points of a trace in the bin. To account for traces that unbind at a point in ΔF, we assume that they unbind uniformly in the interval ΔF and therefore the total time of these traces is given by

$$\frac{1}{2}\delta t \left\langle N_k^{\mathrm{to}} \right\rangle C_k^{\mathrm{un}}. \tag{S 23}$$

Note that the factor 1/2 accounts for the premature unbinding and $\langle N_k^{\mathrm{to}} \rangle$ is the mean number of data points of all traces that pass through the bin.

Taken together, the total time spent in bin k reads

$$\delta t C_k^{\mathrm{to}} = \delta t \left\langle N_k^{\mathrm{to}} \right\rangle \left(\frac{1}{2} C_k^{\mathrm{un}} + \sum_{i=k+1}^{N} C_i^{\mathrm{un}} \right). \tag{S 24}$$

To estimate the loading rate, we approximate the slope of the trace at the center of the bin as constant per bin and obtain

$$\dot{F}_{\mathrm{t}}((k-1/2)\Delta F) = \frac{\Delta F}{\delta t \left\langle N_k^{\mathrm{to}} \right\rangle}, \tag{S 25}$$

from which we get

$$\delta t \left\langle N_k^{\mathrm{to}} \right\rangle = \frac{\Delta F}{\dot{F}_{\mathrm{t}}((k-1/2)\Delta F)}. \tag{S 26}$$

Combining Eq. S 26, Eq. S 24, Eq. S 20 and Eq. S 19, we derive the estimator for the unbinding rate as

$$\epsilon((k-0.5)\Delta F) = \frac{\dot{F}_{\mathrm{t}}((k-1/2)\Delta F) h_k}{\Delta F (h_k/2 + \sum_{i=k+1}^{N} h_i)}, \tag{S 27}$$

which is the estimator proposed by Dudko.[6]

To obtain the unbinding rate with the trace-based method, we cut all traces at their unbinding events. We then bin all points of all traces according to their force and determine the number C_k^{to} of data points in each bin k. The number C_k^{un} of unbinding events readily

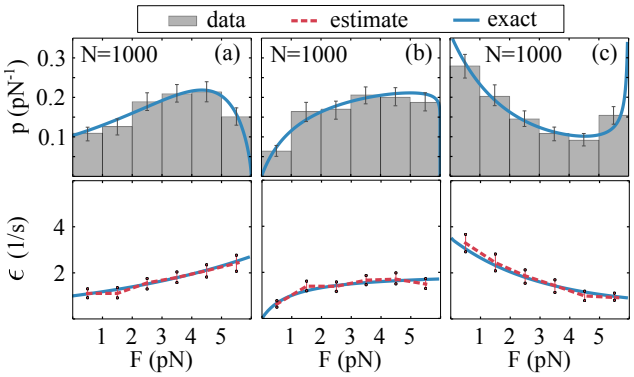

Figure S3: **Validation of the trace-based method with noise-free data** From noise-free simulations we obtain data sets for the three different bond types: (a) the slip bond, (b) the slip-ideal bond, and (c) the catch bond. The probability densities estimated by normalized histograms agree very well with the exact expressions (upper panels). Applying the trace-based method, we accurately determine the underlying force-dependent unbinding rates (lower panels). Each data set consists of $N = 1000$ traces and the error bars are estimated from a bootstrapping procedure as described below.

follows from binning the set of unbinding forces. Together with the inverse sampling rate δt^{-1}, we obtain an estimate for the force-dependent unbinding rate from Eq. S 19.

Validation with noise-free data

To investigate the role of noise and uncertainty, we simulate all three bonds, as parameterized in Table S1, without noise and strictly exclude the parts of the traces, in which the motor is not bound. Using $N = 1000$ traces, we obtain a very good agreement between the data and the exact underlying functions for the distributions, as well as for the force-dependent unbinding rates, see Fig. S3.

The smaller data sets with noise used in the main text display a discrepancy between the simulations and the theory for small forces. This deviation originates from two sources. First, unbinding events that are in the noise floor, smaller than $\sim 0.5\,\mathrm{pN}$, are not detected. Second, the exact time when the motor binds to the filament is unknown. Because of this uncertainty, the data necessarily include parts of the traces around zero force, in which the

motor is not bound and thus we vastly overestimate the number of points C_1^{to} of traces in the first force bin. From Eq.6 of the main text it follows that overestimating C_1^{to} results in an underestimation of the force-dependent unbinding rate as evident in Fig.3 of the main text.

A comparison of the distributions in Fig. S3 to the one shown in Fig.2 of the main text, suggests that the data for the slip bond is more sensitive to noise and the sample size. While the histograms of the slip-ideal and the catch bond in Fig.2 of the main text represent the distributions quite well, the histogram constructed from the slip-bond data underestimates the distribution for forces larger than 4 pN. This underestimation is a result of noise and the small sample size. An underestimation of the tail of the distribution implies an overestimation of the unbinding rate —it is more likely for the motor to unbind at small forces—, see Fig.2 in the main text.

Kinesin-1 data

To determine the force-dependent unbinding rate for kinesin-1, we cut out 682 single unbinding events together with the raising pulling phase. We apply the trace-based method to this data set as explained in the proceeding section. The results are discussed in the main text of the manuscript. To apply the distribution-based method to the experimental data, we determine the cumulative distribution for the slip bond by combining Eq. S 5 and Eq. S 15. For the fitting procedure we evaluate the integrals at 10 equidistant sample points, see blue dots in Fig. S2. We obtain the following optimal parameters with their 95% confidence intervals in brackets: $F_{\mathrm{c}} \simeq 15.62\,[11.26; 18.9]\,\mathrm{pN}$, $F_{\mathrm{d}} \simeq 2.25\,[2.03; 5.18]\,\mathrm{pN}$ and $F_{\mathrm{s}} \simeq 14.97\,[6.26; 15]\,\mathrm{pN}$. However, this fit implies a smaller detachment force compared to the estimate obtained from the trace-based approach and a larger stall force of about 15 pN more than twice the typical kinesin value of $6 - 7\,\mathrm{pN}$.[3,7,8]

In our analysis of the kinesin-1 data, we neglect complex behavior arising from a nonlinear force-velocity relation, from a nonlinear stiffness of the molecule or from heterogeneity of the motor function.[3,9] Kinesin's nonlinear force-velocity relation is almost constant for up to $2-3\,\mathrm{pN}$. A signature of such an initially constant velocity is evident in the constant slop of the trace shown in Fig.4c of the main text. By increasing the stall force F_s of a linear force-velocity relation and thereby decreasing the slope $1/F_\mathrm{s}$, an initially constant force-velocity relation can be approximated. However, such a linear approximation overestimates the velocity for larger forces. Because the distribution is determined by the ratio $\epsilon(F)/\dot{F}_\mathrm{t} = \epsilon(F)/\kappa_\mathrm{eff} v(F)$ (see, Eq. 2, main text) an overestimation of the velocity can be compensated by an overestimated unbinding rate. Thus, our optimization algorithm is trying to increase the stall force to match the nonlinear force-velocity relation and at the same time it increases $\epsilon(F)$ to keep the ratio $\epsilon(F)/\dot{F}_\mathrm{t}$ optimal, in such a way that it fits the distribution. By neglecting nonlinearities in the model for the distribution-based method, we expect that the stall force is overestimated and the detachment force is underestimated.

To determine the force-free unbinding rate ϵ_0 from Eq. S 4, we use the experimental values $v_0 \simeq 484\,\mathrm{nm/s}$ and $\kappa_\mathrm{t} \simeq 0.03\,\mathrm{pN/nm}$.[10] The stiffness of the molecular motor is not a crucial parameter, because the effective stiffness of the motor and the trap is governed by the smaller trap stiffness. We assume a numerical value of $\kappa_\mathrm{m} \simeq 0.3\,\mathrm{pN/nm}$.[3] With these parameter values, we obtain the force-free unbinding rate $\epsilon_0 \simeq 0.97\,[0.80; 1.35]\,\mathrm{s}^{-1}$.

Estimation of variability

Distribution-based method

To illustrate the variability of the data, we resample 200 data sets of the unbinding events and apply the fitting procedure. From each calculation we obtain a force-dependent unbinding rate. In Fig.2 and Fig.4 of the main text, we display the 95% of the closest unbinding rates

as thin gray lines in the background. The error bars for the histograms are determined as the 2.5 percentile and the 97.5 percentile of the data from a bootstrapping procedure with 200 resamples and the same number of unbinding forces as in the original data set.

Trace-based method

To determine the 95% confidence intervals at a significance of 0.05, we use a bootstrapping approach. We resample 200 data sets of unbinding events with the corresponding traces of the original size. For each data set we determine the unbinding rate from Eq. S 19. Thus, we have for each sampling point of the force 200 different numerical values for the unbinding rate. We then calculate the lower and upper confidence interval as the 2.5 percentile and the 97.5 percentile of the unbinding rates at each force step.

References

(1) Dembo, M. *Lectures on Mathematics in the Life Sciences, Some Mathematical Problems in Biology*; American Mathematical Society: Providence, RI, 1994; 51–77.

(2) Nicholas, M. P.; Berger, F.; Rao, L.; Brenner, S.; Cho, C.; Gennerich, A. *Proc. Natl. Acad. Sci. U.S.A.* **2015**, *112*, 6371–6376.

(3) Coppin, C. M.; Pierce, D. W.; Hsu, L.; Vale, R. D. *Proc. Natl. Acad. Sci. U.S.A.* **1997**, *94*, 8539–8544.

(4) Gillespie, D. T. *J. Phys. Chem.* **1977**, *81*, 2340–2361.

(5) Thorn, K. S.; Ubersax, J. A.; Vale, R. D. *J. Cell. Biol.* **2000**, *151*, 1093–1100.

(6) Dudko, O. K.; Hummer, G.; Szabo, A. *Proc. Natl. Acad. Sci. U.S.A.* **2008**, *105*, 15755–15760.

(7) Carter, N. J.; Cross, R. A. *Nature* **2005**, *435*, 308–312.

(8) Andreasson, J. O.; Milic, B.; Chen, G.; Guydosh, N. R.; Hancock, W. O.; Block, S. M. *eLife* **2015**, *4*, e07403.

(9) Reddy, B. J.; Tripathy, S.; Vershinin, M.; Tanenbaum, M. E.; Xu, J.; Mattson-Hoss, M.; Arabi, K.; Chapman, D.; Doolin, T.; Hyeon, C.; Gross, S. P. *Traffic* **2017**, *18*, 658–671.

(10) DeBerg, H. A.; Blehm, B. H.; Sheung, J.; Thompson, A. R.; Bookwalter, C. S.; Torabi, S. F.; Schroer, T. A.; Berger, C. L.; Lu, Y.; Trybus, K. M.; Selvin, P. R. *J. Biol. Chem.* **2013**, *288*.